

# Applications of Skyrme energy-density functional to fusion reactions for synthesis of superheavy nuclei

Ning Wang,<sup>1,\*</sup> Xizhen Wu,<sup>2</sup> Zhuxia Li,<sup>2,3,4</sup> Min Liu,<sup>2</sup> and Werner Scheid<sup>1</sup>

<sup>1</sup>*Institute for Theoretical Physics at Justus-Liebig-University, D-35392 Giessen, Germany*

<sup>2</sup>*China Institute of Atomic Energy, Beijing 102413, P. R. China*

<sup>3</sup>*Institute of Theoretical Physics, Chinese Academy of Science, Beijing 100080, P. R. China*

<sup>4</sup>*Nuclear Theory Center of National Laboratory of Heavy Ion Accelerator, Lanzhou 730000, P. R. China*

(Dated: October 20, 2018)

## Abstract

The Skyrme energy-density functional approach has been extended to study the massive heavy-ion fusion reactions. Based on the potential barrier obtained and the parameterized barrier distribution the fusion (capture) excitation functions of a lot of heavy-ion fusion reactions are studied systematically. The average deviations of fusion cross sections at energies near and above the barriers from experimental data are less than 0.05 for 92% of 76 fusion reactions with  $Z_1 Z_2 < 1200$ . For the massive fusion reactions, for example, the  $^{238}\text{U}$ -induced reactions and  $^{48}\text{Ca}+^{208}\text{Pb}$  the capture excitation functions have been reproduced remarkable well. The influence of structure effects in the reaction partners on the capture cross sections are studied with our parameterized barrier distribution. Through comparing the reactions induced by double-magic nucleus  $^{48}\text{Ca}$  and by  $^{32}\text{S}$  and  $^{35}\text{Cl}$ , the 'threshold-like' behavior in the capture excitation function for  $^{48}\text{Ca}$  induced reactions is explored and an optimal balance between the capture cross section and the excitation energy of the compound nucleus is studied. Finally, the fusion reactions with  $^{36}\text{S}$ ,  $^{37}\text{Cl}$ ,  $^{48}\text{Ca}$  and  $^{50}\text{Ti}$  bombarding on  $^{248}\text{Cm}$ ,  $^{247,249}\text{Bk}$ ,  $^{250,252,254}\text{Cf}$  and  $^{252,254}\text{Es}$ , and as well as the reactions lead to the same compound nucleus with  $Z = 120$  and  $N = 182$  are studied further. The calculation results for these reactions are useful for searching for the optimal fusion configuration and suitable incident energy in the synthesis of superheavy nuclei.

---

\*Electronic address: Ning.Wang@theo.physik.uni-giessen.de

## I. INTRODUCTION

It is of great importance to predict fusion cross sections and to analyze reaction mechanism for massive heavy-ion fusion reactions, especially for fusion reactions leading to superheavy nuclei. In those reactions, the calculation of the capture cross section is of crucial importance. It is known that Wong's formula[1] based on one-dimensional barrier penetration can describe the fusion excitation function well for light reaction systems, while it fails to give satisfying results for heavy reaction systems at energies near and below the barrier. For solving this problem, a fusion coupled channel model [2] was proposed, in which the macroscopic Woods-Saxon potential together with a microscopic channel coupling concept is adopted. By this model fusion excitation functions of some reactions at energies near and below the barrier are successfully described. However, it has been found that the parameters in the Woods-Saxon potential greatly influence on the results [3] and for heavy systems the potential parameters need to be readjusted in order to reproduce experimental data [4]. How to determine the parameters is still an open problem for predicting fusion cross sections of unmeasured reaction systems. Therefore, it is highly requisite to propose a new method for systematically describing fusion reactions from light to heavy reaction systems.

In our previous paper[5], we applied the Skyrme energy-density functional for the first time to study heavy-ion fusion reactions. The barrier for fusion reaction was calculated by the Skyrme energy-density functional together with the semi-classical extended Thomas-Fermi method[6]. Based on the interaction potential barrier obtained, we proposed a parametrization of the empirical barrier distribution to take into account the multi-dimensional character of the real barrier and then applied it to calculate the fusion excitation functions of light and intermediate-heavy fusion reaction systems in terms of the barrier penetration concept. A large number of measured fusion excitation functions at energies around the barriers were reproduced well. Now we try to extend this approach to study very heavy fusion reaction systems which may lead to the formation of superheavy nuclei. In these cases, the reaction mechanism is very complicated and the capture process is the firstly concerned process, which follows by the quasi-fission and fusion, and then the fused system further undergoes fusion-fission and evaporation.

The study of the fusion mechanism (or capture process in very heavy fusion systems), especially of the possible enhancement of the fusion (capture) cross section in neutron-

rich reactions and also of the suppression of fusion (capture) cross section induced by the strong shell effects of projectile or target, is very interesting and essentially importance for the synthesis of superheavy nuclei. For fusion reactions induced by double-magic nucleus  $^{48}\text{Ca}$ , there exists a puzzle: on one hand, it has been found that the fusion cross sections at sub-barrier energies are suppressed in fusion reactions  $^{48}\text{Ca}+^{48}\text{Ca}$ [7] and  $^{48}\text{Ca}+^{90,96}\text{Zr}$  [8, 9] compared with the  $^{40}\text{Ca}+^{48}\text{Ca}$  and  $^{40}\text{Ca}+^{90,96}\text{Zr}$ , respectively. On the other hand, the experiments of production of superheavy elements  $Z = 114$  and  $116$  in "hot fusion" reactions with  $^{48}\text{Ca}$  bombarding Pu and Cm targets[10] indicate that the reactions with  $^{48}\text{Ca}$  nuclei, indeed, are quite favorable for the synthesis of superheavy nuclei. Therefore, it is worthwhile to explore the puzzle concerning the fusion reactions induced by  $^{48}\text{Ca}$ . For this purpose, the influence of shell structure, that is, the influence of the Q-value in fusion (capture) process on the fusion (capture) cross section is considered in our approach. The choice of an optimal reaction combination and a suitable incident energy is always of crucial importance for the synthesis of new superheavy nuclei. In order to choose a suitable incident energy, an optimal balance between capture cross section and excitation energy of compound nuclei should be taken into account. Thus, in this work, a series of fusion reactions induced by  $^{48}\text{Ca}$ ,  $^{36}\text{S}$ ,  $^{37}\text{Cl}$  and  $^{50}\text{Ti}$  are investigated within our approach and the optimal incident energies for the reactions are given.

## II. MICROSCOPIC INTERACTION POTENTIAL BARRIER AND PARAMETERIZED BARRIER DISTRIBUTION

In this section, we briefly introduce our approach for calculating the interaction potential barrier and fusion (capture) excitation function, a more detailed description can be found in ref.[5]. The nucleus-nucleus interaction potentials of fusion systems are calculated within the microscopic Skyrme energy-density functional together with the semi-classical extended Thomas-Fermi (ETF2) approach (up to second order of  $\hbar$ ). The interaction potential  $V_b(R)$  between reaction partners can be written as

$$V_b(R) = E_{tot}(R) - E_1 - E_2, \quad (1)$$

where  $R$  is the center-to-center distance between reaction partners,  $E_{tot}(R)$  is the total energy of the interaction system,  $E_1$  and  $E_2$  are the energies of the non-interacting projectile and target, respectively. The interaction potential  $V_b(R)$  is also called the entrance-channel

potential in ref.[11] or fusion potential in ref.[12]. The  $E_{tot}(R)$ ,  $E_1$ ,  $E_2$  are determined by the Skyrme energy-density functional[6, 11, 13, 14, 15],

$$E_{tot}(R) = \int \mathcal{H}[\rho_{1p}(\mathbf{r}) + \rho_{2p}(\mathbf{r} - \mathbf{R}), \rho_{1n}(\mathbf{r}) + \rho_{2n}(\mathbf{r} - \mathbf{R})] d\mathbf{r}, \quad (2)$$

$$E_1 = \int \mathcal{H}[\rho_{1p}(\mathbf{r}), \rho_{1n}(\mathbf{r})] d\mathbf{r}, \quad (3)$$

$$E_2 = \int \mathcal{H}[\rho_{2p}(\mathbf{r}), \rho_{2n}(\mathbf{r})] d\mathbf{r}. \quad (4)$$

Here,  $\rho_{1p}$ ,  $\rho_{2p}$ ,  $\rho_{1n}$  and  $\rho_{2n}$  are the frozen proton and neutron densities of the projectile and target, and the expression of the energy-density functional  $\mathcal{H}$  can be found in refs.[5, 11]. Once the proton and neutron density distributions of the projectile and target are determined, the interaction potential  $V_b(R)$  can be calculated from eqs.(1) – (4).

By density-variational approach and minimizing the total energy of a single nucleus given by the Skyrme energy-density functional  $\mathcal{H}$ , the neutron and proton densities of this nucleus can be obtained. In this work we take the neutron ( $i = n$ ) and proton ( $i = p$ ) density distributions of nuclei as spherical symmetric Fermi functions,

$$\rho_i(\mathbf{r}) = \rho_{0i} \left[ 1 + \exp \left( \frac{r - R_{0i}}{a_i} \right) \right]^{-1}, \quad i = \{n, p\}. \quad (5)$$

Only two of the three quantities  $\rho_{0i}$ ,  $R_{0i}$  and  $a_i$  in this relation, are independent because of the conservation of the particle numbers  $N_i = \int \rho_i(\mathbf{r}) d\mathbf{r}$ ,  $N_i = \{N, Z\}$ . For example,  $\rho_{0p}$  can be expressed as a function of  $R_{0p}$  and  $a_p$ ,

$$\rho_{0p} \simeq Z \left\{ \frac{4}{3} \pi R_{0p}^3 \left[ 1 + \pi^2 \left( \frac{a_p}{R_{0p}} \right)^2 \right] \right\}^{-1} \quad (6)$$

with high accuracy[16] when  $R_{0p} \gg a_p$ . By using an optimization algorithm, one can obtain the minimal energy and the corresponding  $R_{0p}$ ,  $a_p$ ,  $R_{0n}$ ,  $a_n$  for neutron and proton densities. Then, with the neutron and proton densities of projectile and target obtained we can calculate the entrance-channel potential with the same energy-density functional. For systematically investigating massive heavy-ion fusion reactions with a simple self-consistent manner provided by the density functional theory[17], an optimal balance between the accuracy and computation cost is adopted in this approach, which is especially valuable for these cases.

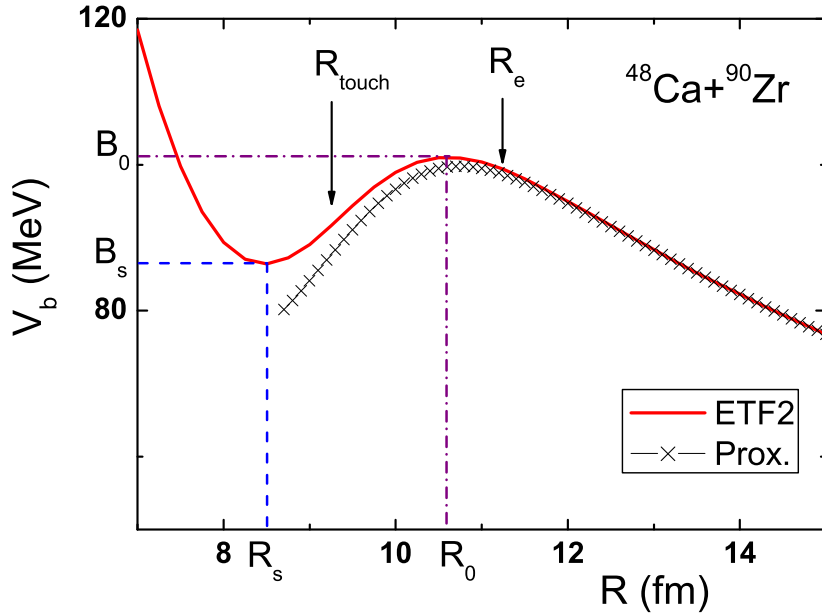


FIG. 1: (Color online) The entrance-channel potential for reaction  $^{48}\text{Ca}+^{90}\text{Zr}$ .

The Skyrme force SkM\*[15] is adopted in this work. For a certain reaction system, the entrance-channel potential is calculated in a range from  $R = 7\text{ fm}$  to  $15\text{ fm}$  with a step size  $\Delta R = 0.25\text{ fm}$ . Fig.1 shows the entrance-channel potential of  $^{48}\text{Ca}+^{90}\text{Zr}$ . The solid and crossed curves denote the results of this approach and of the proximity potential[18], respectively. The results of Skyrme energy-density functional approach are generally close to those of proximity potential in the region where the densities of the two nuclei do not overlap. The barrier height  $B_0$ , radius  $R_0$  and the curvature  $\hbar\omega_0$  near  $R_0$  as well as the position of fusion pocket  $R_s$  can be obtained from the calculations (see Fig.1). Here, the curvature  $\hbar\omega_0$  of the barrier is obtained through fitting the entrance-channel potential in the region from  $R_0 - 1.25\text{ fm}$  to  $R_0 + 1.25\text{ fm}$  by an inverted parabola (if  $R_0 - 1.25\text{ fm} < R_s$ , then from  $R_s$  to  $R_0 + 1.25\text{ fm}$ ).

To overcome the deficiency of one-dimensional barrier penetration model for describing sub-barrier fusion of heavy systems, we take into account the multi-dimensional character of realistic barrier[19] due to the coupling to internal degrees of freedom of the binary system. We assume that the one-dimensional barrier is replaced by a distribution of fusion barrier

$D(B)$ . The distribution function  $D(B)$  satisfies:

$$\int_0^\infty D(B)dB = 1. \quad (7)$$

Motivated by the shape of the barrier distribution extracted from experiments, we consider the weighting function to be a superposition of two Gaussian functions  $D_1(B)$  and  $D_2(B)$ , which read

$$D_1(B) = \frac{\sqrt{\gamma}}{2\sqrt{\pi}w_1} \exp \left[ -\gamma \frac{(B - B_1)^2}{(2w_1)^2} \right] \quad (8)$$

and

$$D_2(B) = \frac{1}{2\sqrt{\pi}w_2} \exp \left[ -\frac{(B - B_2)^2}{(2w_2)^2} \right], \quad (9)$$

with

$$w_1 = \frac{1}{4}(B_0 - B_c), \quad (10)$$

$$w_2 = \frac{1}{2}(B_0 - B_c), \quad (11)$$

$$B_1 = B_c + w_1, \quad (12)$$

$$B_2 = B_c + w_2. \quad (13)$$

Here  $B_0$  is the height of the barrier (see Fig.1). The  $B_c = fB_0$  is the effective barrier height with a reducing factor  $f$  to mimic the lowering barrier effect which is due to the coupling to other degrees of freedom, such as dynamical deformation and nucleon transfer, etc. We set the reducing factor  $f = 0.926$  in this work, which is the same as in [5]. The quantity  $\gamma$  in  $D_1(B)$  is a factor to taken into account the structure effects, which influences the width of the distribution  $D_1(B)$ . For the fusion reactions with non-closed-shell nuclei but near the  $\beta$ -stability line we set  $\gamma = 1$ ; for fusion reactions with neutron-shell-closed nuclei or neutron-rich nuclei an empirical formula for the  $\gamma$  values, used in the weighting function  $D_1(B)$  for systems with the same  $Z_1$  and  $Z_2$ , was proposed in ref.[5] as

$$\gamma = 1 - c_0\Delta Q + 0.5(\delta_n^{prog} + \delta_n^{targ}), \quad (14)$$

where  $\Delta Q = Q - Q_0$  denotes the difference between the Q-values of the system under considering for complete fusion and that of the reference system. The reference system, in general, is chosen to be the reaction system with nuclei along the  $\beta$ -stability line [5]. The value of  $c_0$  is  $0.5 \text{MeV}^{-1}$  for  $\Delta Q < 0$  and  $0.1 \text{MeV}^{-1}$  for  $\Delta Q > 0$ . The quantities  $\delta_n^{proj(targ)}$  are 1 for neutron closed-shell projectile (target) nucleus and 0 for non-closed cases.

The fusion excitation function is then given by

$$\sigma_f(E_{\text{c.m.}}) = \int_0^\infty D(B) \sigma_{fus}^{\text{Wong}}(E_{\text{c.m.}}, B) dB, \quad (15)$$

with

$$\sigma_{fus}^{\text{Wong}}(E_{\text{c.m.}}, B) = \frac{\hbar\omega_0 R_0^2}{2E_{\text{c.m.}}} \ln \left( 1 + \exp \left[ \frac{2\pi}{\hbar\omega_0} (E_{\text{c.m.}} - B) \right] \right), \quad (16)$$

where  $E_{\text{c.m.}}$  denotes the center-of-mass energy, and  $B$ ,  $R_0$  and  $\hbar\omega_0$  are the barrier height, radius and curvature, respectively. Using the parameterized barrier distribution functions  $D_1(B)$  and  $D_2(B)$ , we also can obtain the cross sections  $\sigma_1(E_{\text{c.m.}})$  and  $\sigma_{\text{avr}}(E_{\text{c.m.}})$  by (15) with  $D(B)$  taken to be  $D_1(B)$  and  $D_{\text{avr}}(B) = [D_1(B) + D_2(B)]/2$ , respectively. Finally, the fusion cross section is given by

$$\sigma_{fus}(E_{\text{c.m.}}) = \min[\sigma_1(E_{\text{c.m.}}), \sigma_{\text{avr}}(E_{\text{c.m.}})]. \quad (17)$$

The cross section calculated with (17) is referred to as fusion cross section for a light and intermediate-heavy system and as capture cross section for a very heavy system at  $E_{\text{c.m.}}$ .

### III. CALCULATED RESULTS FOR FUSION (CAPTURE) EXCITATION FUNCTIONS

In order to extend our approach to study the fusion reactions leading to superheavy nuclei, we first check the suitability and reliability of our description of heavy-ion fusion reactions. We calculate the fusion excitation functions of 76 fusion reactions with  $Z_1 Z_2 < 1200$  at energies near and above the barrier (with  $\gamma = 1$ ) and their average deviations  $\chi_{\log}^2$  from experimental data defined as

$$\chi_{\log}^2 = \frac{1}{m} \sum_{n=1}^m [\log(\sigma_{th}(E_n)) - \log(\sigma_{exp}(E_n))]^2. \quad (18)$$

Here  $m$  denotes the number of energy-points of experimental data, and  $\sigma_{th}(E_n)$  and  $\sigma_{exp}(E_n)$  are the calculated and experimental fusion cross sections at the center-of-mass energy  $E_n$

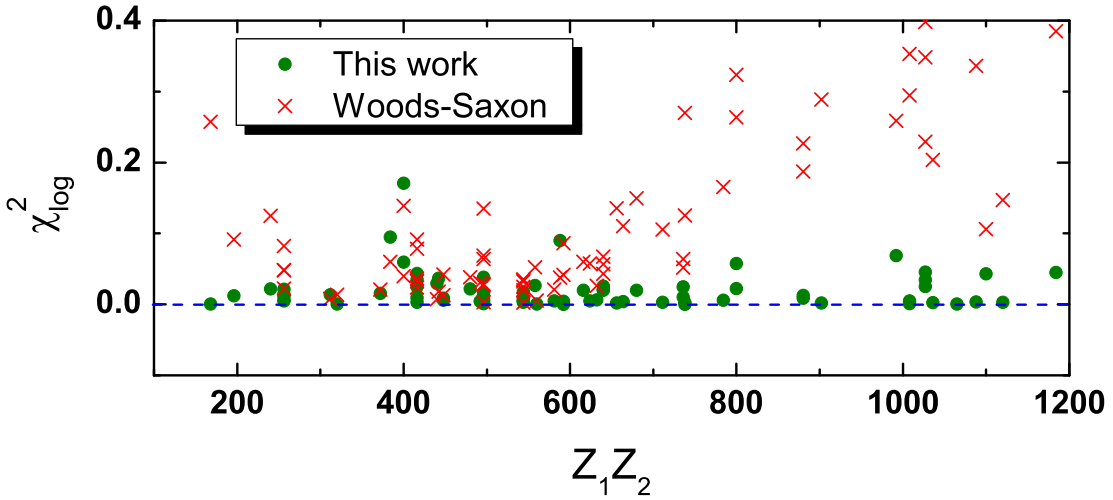


FIG. 2: (Color online) The average deviations  $\chi_{\log}^2$  for a total of 76 fusion reactions with  $Z_1Z_2 < 1200$ . The solid circles and crosses denote the results of our approach and those with a Woods-Saxon potential with fixed potential parameters[2], respectively. In the calculations of fusion cross sections at energies near and above the barrier with the Woods-Saxon potential, the code CCFULL[2] is used without taking into account the excitation and deformation of the reaction partners.

$(E_n \geq B_0)$ , respectively. Fig.2 shows the results for  $\chi_{\log}^2$  in which the solid circles and crosses denote the calculated results from this approach and those from ref.[2], respectively. Applying the approach of ref.[2] there are 43% systems in 76 fusion reactions in which the average deviations  $\chi_{\log}^2$  of calculated fusion cross sections from the experimental data are less than 0.05, but for reactions with  $Z_1Z_2 > 640$  the results are not satisfying very well. With our approach, the average deviations of 92% systems in  $\chi_{\log}^2$  are less than 0.05, which indicates that this approach is successful for describing fusion cross sections of heavy-ion reactions at energies near and above the barrier from light to intermediate-heavy fusion systems. In Fig.3 we show three examples of fusion excitation functions for the reactions  $^{16}\text{O}+^{144}\text{Sm}$ [20],  $^{16}\text{O}+^{92}\text{Zr}$ [21] and  $^{64}\text{Ni}+^{92}\text{Zr}$ [22], in which the solid and dashed curves present the results of our approach and of ref.[2], respectively, the squares denote the experimental data. From this figure we can see that our approach gives quite reasonable description for all selected fusion reactions with the  $Z_1Z_2$  up to 1120 at energies near and above the barrier.

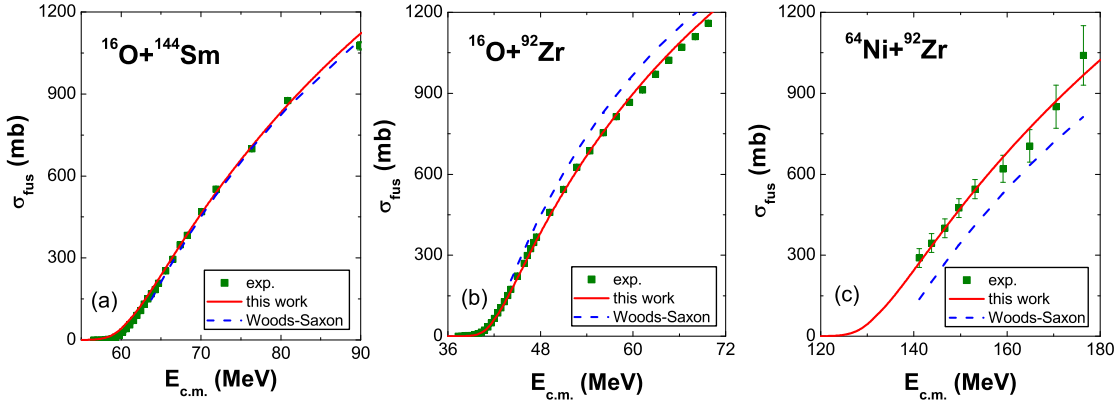


FIG. 3: (Color online) Fusion excitation functions for  $^{16}\text{O} + ^{144}\text{Sm}$ ,  $^{16}\text{O} + ^{92}\text{Zr}$  and  $^{64}\text{Ni} + ^{92}\text{Zr}$ . The squares and solid curves denote the experimental data and the results of this work, respectively. The dashed curves denote the results of the approach with the Woods-Saxon potential with fixed potential parameters[2].

For more massive fusion reactions leading to superheavy nuclei, the quasi-fission process occurs and therefore, the capture cross sections are larger than the corresponding fusion cross sections. In ref.[23] the fission and quasi-fission process in  $^{238}\text{U}$ -induced reactions were studied. Fig.4 shows the results in which the solid and open circles denote the measured cross sections for the fission-like process and for complete fusion followed by fission, respectively. The solid curves give the calculated results of our approach with  $\gamma = 1$ . From this figure one can see that the calculated capture excitation functions of the reactions  $^{238}\text{U} + ^{26}\text{Mg}$ ,  $^{238}\text{U} + ^{27}\text{Al}$ ,  $^{238}\text{U} + ^{32}\text{S}$ , and  $^{238}\text{U} + ^{35}\text{Cl}$  are quite close to the measured fission-like cross sections. It implies that our approach can describe the massive fusion reactions between nuclei with neutron open shells but near the  $\beta$ -stability line.

For the very massive fusion reaction between double-magic nuclei  $^{48}\text{Ca}$  and  $^{208}\text{Pb}$ , the influence of the shell effects is very significant. So careful consideration of the  $\gamma$  value is required at sub-barrier energies. Fig.5 shows the calculated capture excitation function of  $^{48}\text{Ca} + ^{208}\text{Pb}$  and the experimental data of refs.[25] and [26]. The dashed curve presents the results with  $\gamma = 1$ , that is, no neutron-shell-closure effect is considered. The solid curve is calculated with  $\gamma = 9.5$  according to eq.(14), in which the closed shell effect is considered.

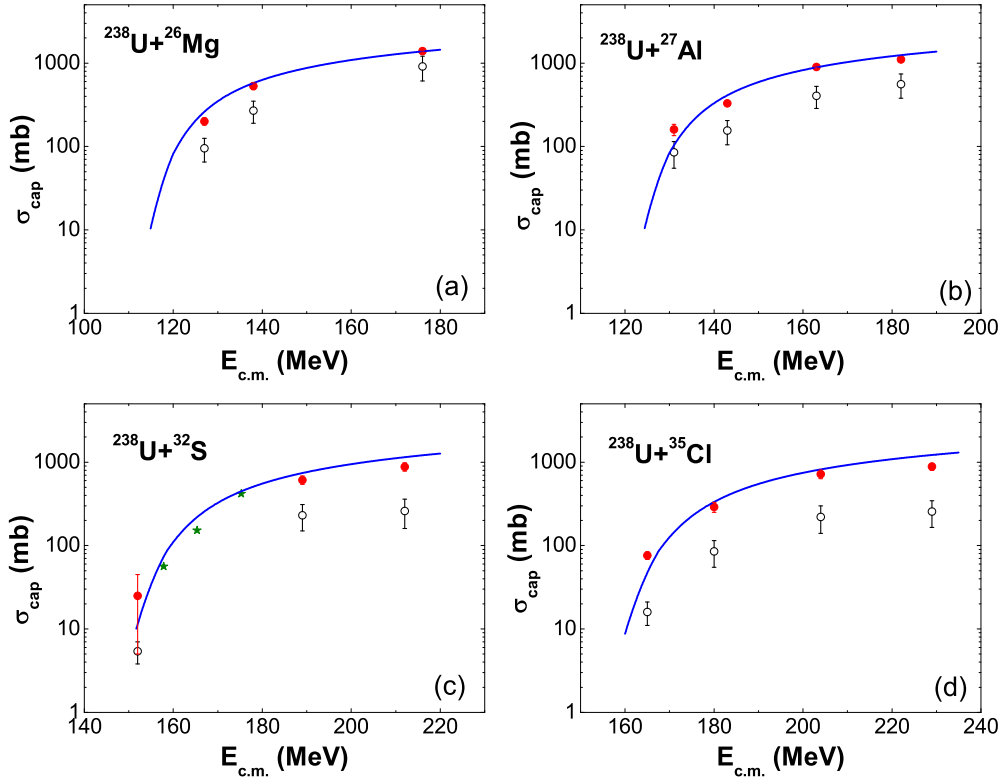


FIG. 4: (Color online) Capture cross sections of  $^{238}\text{U}+^{26}\text{Mg}$ ,  $^{27}\text{Al}$ ,  $^{32}\text{S}$ ,  $^{35}\text{Cl}$ . The solid and open circles denote the measured cross sections for a fission-like process and for complete fusion followed by fission, respectively. The solid curves are the results from our approach with  $\gamma = 1$ . The stars are taken from ref.[24].

We find that for energies below the barrier the experimental data can only be described with  $\gamma = 9.5$  and the calculations with  $\gamma = 1$  are over-predicted. From this analysis, one learns that the measured capture cross sections of  $^{48}\text{Ca}+^{208}\text{Pb}$  at sub-barrier energies are obviously suppressed, which may arise from the suppression of the nucleon transfer between reaction partners due to the strong closed shell effects, which will be further studied in the following section.

#### IV. OPTIMAL BALANCE BETWEEN CAPTURE CROSS SECTION AND EXCITATION ENERGY OF COMPOUND NUCLEI

It is very important to find a favorable combination of projectile and target and a suitable

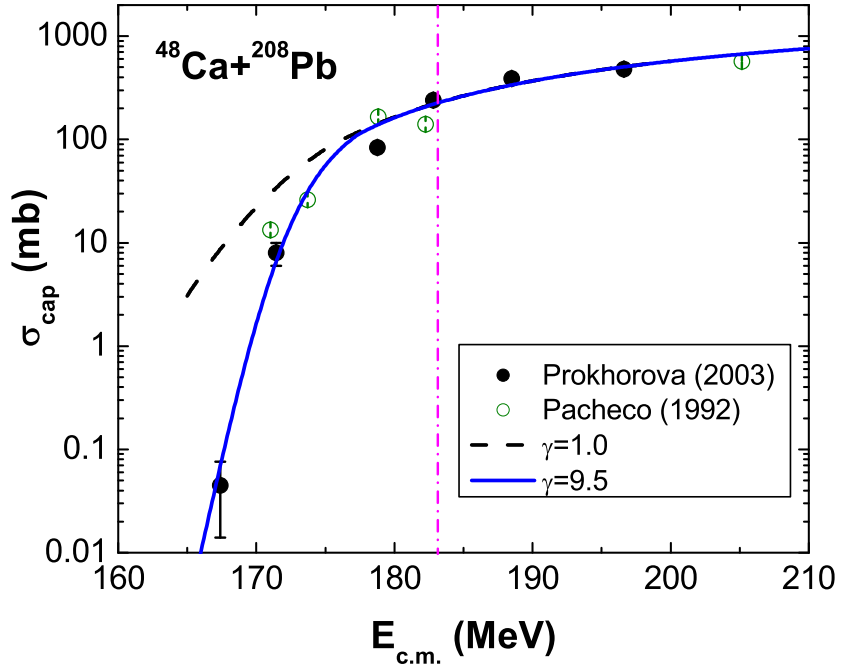


FIG. 5: (Color online) Capture cross sections of  $^{48}\text{Ca} + ^{208}\text{Pb}$ . The solid and open circles denote the measured capture-fission cross sections from ref.[25] and ref.[26], respectively. The dashed and solid curves present the calculated results with  $\gamma = 1.0$  and  $9.5$  obtained by eq.(14), respectively. The dash-dotted line indicates the energy corresponding to the height of the barrier.

incident energy for synthesis of superheavy nuclei. In this section we study very massive fusion reactions and search for an optimal balance between the capture cross section in the entrance channel and the excitation energy of the compound nuclei. For searching a fusion system with large capture cross sections, we carried out a series of calculations for fusion reactions induced by  $^{32,36}\text{S}$ ,  $^{35,37}\text{Cl}$  and  $^{48}\text{Ca}$  projectiles. For example, Fig.6 shows the capture excitation functions of the reactions  $^{32}\text{S} + ^{254}\text{Cf}$  and  $^{35}\text{Cl} + ^{254}\text{Es}$ . The solid curves present the results with  $\gamma = 1$  (without considering structure effects in the entrance channel), and the dashed curves are for the results with the  $\gamma$  obtained from (14) i.e.  $\gamma = 0.5$  for  $^{32}\text{S} + ^{254}\text{Cf}$  and  $\gamma = 0.6$  for  $^{35}\text{Cl} + ^{254}\text{Es}$ . The enhancement of capture cross sections in the sub-barrier energy region with the  $\gamma < 1$  is caused by the effect of excess of neutrons in reaction systems. So from the point of view of increasing the capture cross sections, it is more favorable to

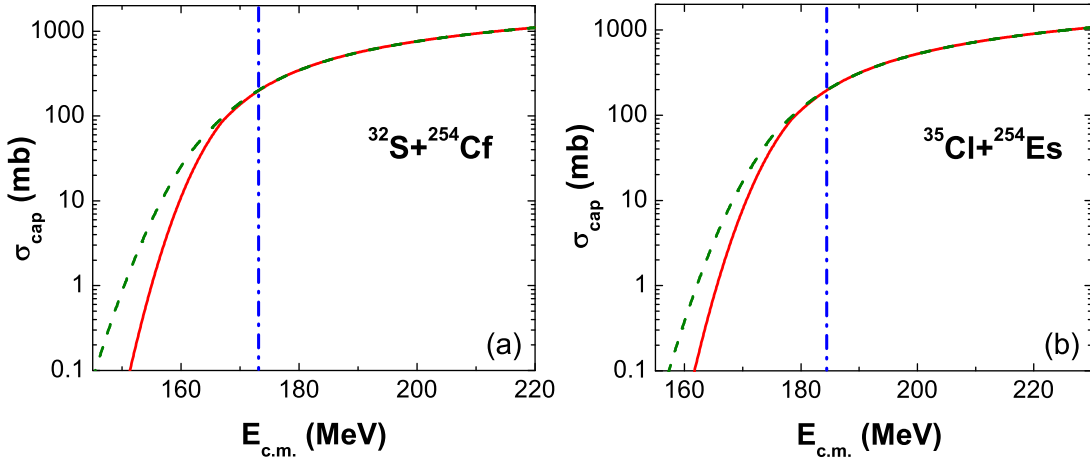


FIG. 6: (Color online) Capture excitation functions for fusion systems  $^{32}\text{S}+^{254}\text{Cf}$  and  $^{35}\text{Cl}+^{254}\text{Es}$ . The dash-dotted lines indicate the corresponding barriers. The solid and dashed curves denote the results with  $\gamma = 1$  and with  $\gamma$  value obtained with eq.(14), respectively.

select the reaction systems with  $\gamma < 1$ . However, the amount of the excitation energy of the formed compound nucleus is essentially important for the survival probability. The smaller the excitation energy is, the larger the surviving probability is. Thus, seeking an optimal balance between the capture cross section and the excitation energy of the compound nucleus becomes very important for synthesis of superheavy nuclei. For choosing the fused nuclei with an excitation energy as low as possible, the fusion reactions with double-magic nuclei  $^{48}\text{Ca}$  are considered to be good candidates because of the low Q-values for those fusion reactions. As an example, let us investigate reaction  $^{48}\text{Ca}+^{248}\text{Cm}$ . For this reaction the  $\gamma$  value is equal to 10.8 calculated with eq.(14). Fig.7 shows the capture excitation function for this reaction, in which the solid and dashed curves denote the results for the cases of  $\gamma = 1$  and  $\gamma=10.8$ , respectively. From this figure one finds that for fusion reactions induced by double-magic nuclei  $^{48}\text{Ca}$  the capture cross sections at sub-barrier energies are suppressed compared with reactions with shell-open nuclei but near the  $\beta$ -stability line. However, if we suitably choose an incident energy, for example, as indicated by the arrow in Fig.7, the capture cross section of the reaction  $^{48}\text{Ca}+^{248}\text{Cm}$  is not suppressed so much (still reaches several tens of milli-barns) and the excitation energy of the compound nuclei

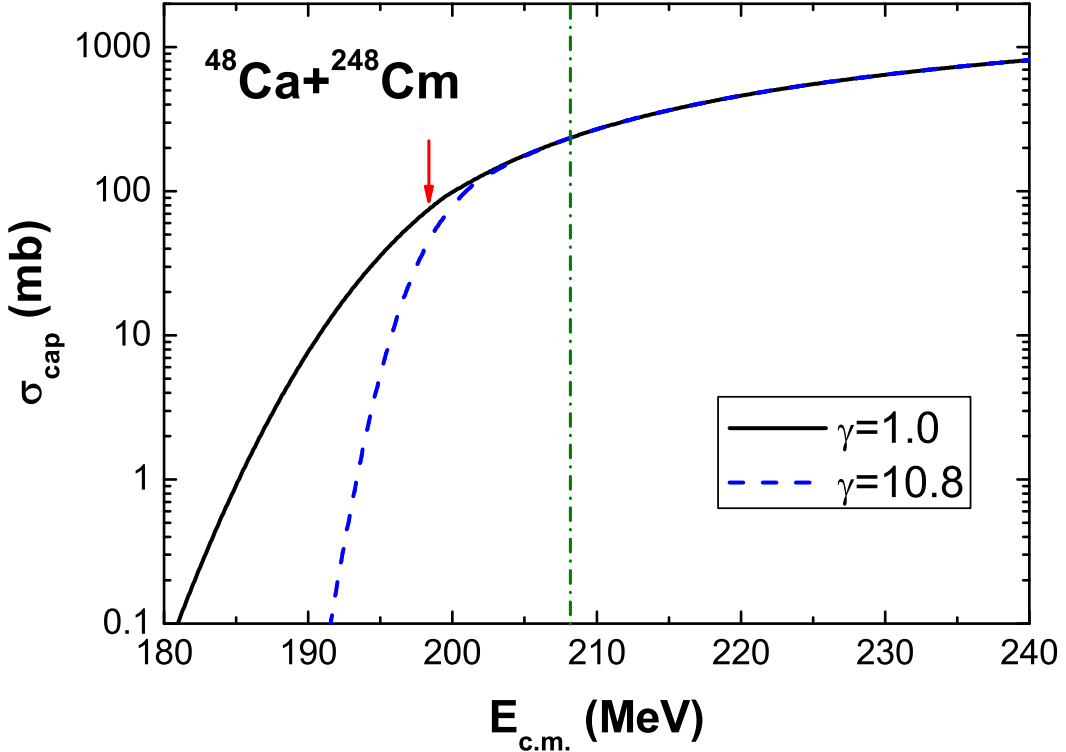


FIG. 7: (Color online) Capture excitation functions for  $^{48}\text{Ca}+^{248}\text{Cm}$ . The solid and dashed curves represent the results with the  $\gamma = 1$  and with  $\gamma = 10.8$  obtained from eq.(14). The arrow indicates the incident energy at which the corresponding excitation energy of the formed compound nucleus is  $E_{CN}^* = 31\text{MeV}$ .

is only  $E_{CN}^* = 31\text{MeV}$ . Such an incident energy was already used in the experiment of ref.[10]. Now let us make a comparison between the reaction  $^{48}\text{Ca}+^{248}\text{Cm}$  and the reactions  $^{32}\text{S}+^{254}\text{Cf}$  and  $^{35}\text{Cl}+^{254}\text{Es}$ . For the system  $^{48}\text{Ca}+^{248}\text{Cm}$ , the capture cross section is of about  $80\text{mb}$  and the excitation energy is about  $31\text{MeV}$  if the incident energy is taken to be about  $198\text{MeV}$ . While, for the systems  $^{32}\text{S}+^{254}\text{Cf}$  and  $^{35}\text{Cl}+^{254}\text{Es}$ , if the same excitation energy is required the incident energies must be as low as about  $150\text{MeV}$  and  $160\text{MeV}$ , respectively, since the Q-values of these two fusion reactions are much higher compared with  $^{48}\text{Ca}$  induced reactions. At these incident energies the capture cross sections for these two reactions are as small as those less than  $0.1\text{mb}$  according to this model calculations. From above analysis we

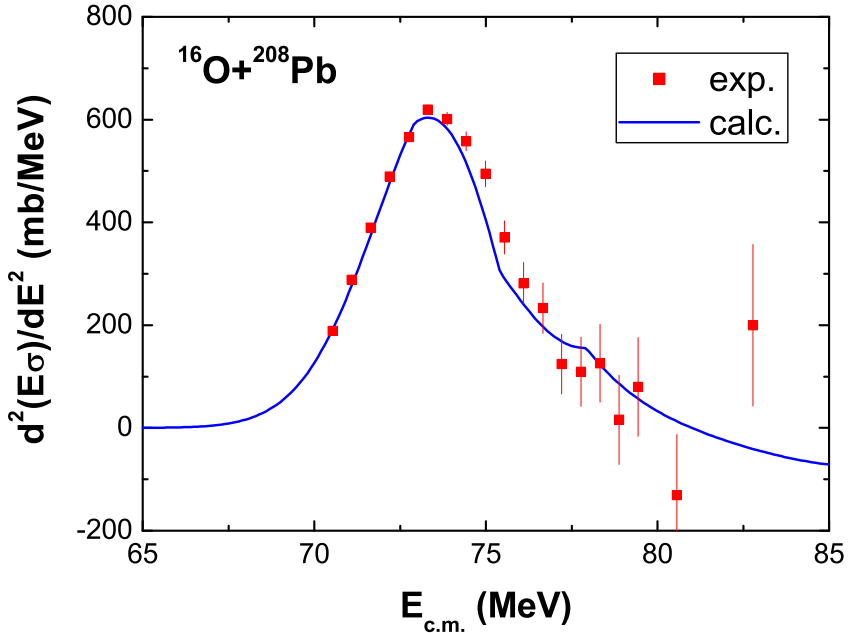


FIG. 8: (Color online) Fusion barrier distribution for  $^{16}\text{O} + ^{208}\text{Pb}$ . The distribution is evaluated with  $\Delta E_{\text{c.m.}} = 2.5\text{MeV}$ . The solid squares and solid curve present the experimental data and the results from our calculations, respectively.

can conclude that the fusion reaction  $^{48}\text{Ca} + ^{248}\text{Cm}$  seems to be more favorable compared to  $^{32}\text{S} + ^{254}\text{Cf}$  and  $^{35}\text{Cl} + ^{254}\text{Es}$  if a suitable incident energy is chosen, as far as both the capture cross section and the excitation energy of the compound nuclei are concerned.

Now let us discuss how to choose suitable incident energy. We notice that the capture excitation function for reactions induced by double-magic  $^{48}\text{Ca}$  goes very sharply down at sub-barrier energies due to strong closed shell effects, as shown by the dashed curve of Fig.7. It seems to us that there exists a 'threshold-like' behavior, which is important for choosing the incident energies. This 'threshold-like' behavior of excitation function of capture cross sections is closely related to the shape of the barrier distribution. In our previous paper [5], a number of barrier distributions were calculated according to expressions (8)-(13). As example, here we show the calculated fusion barrier distribution for  $^{16}\text{O} + ^{208}\text{Pb}$  [31] in Fig.8. The agreement of the calculated barrier distribution with experimental data tells us that our approach about the parameterized barrier distribution is quite reasonable. The effective

weighting function  $D_{\text{eff}}(B)$  is defined as

$$D_{\text{eff}}(B) = \begin{cases} D_1(B) & : B < B_x \\ D_{\text{avr}}(B) & : B \geq B_x \end{cases} \quad (19)$$

(with  $\int D_{\text{eff}}(B) dB \approx 1$  and  $\int D_{\text{avr}}(B) dB = 1$ , see ref.[5]). The  $B_x$  denotes the position of the left crossing point between  $D_1(B)$  and  $D_{\text{avr}}(B)$ . The function  $D_{\text{eff}}(B)$  can describe the fusion excitation function reasonably well. Fig.9 shows the capture excitation function (Fig.9(a)) and the effective weighting function  $D_{\text{eff}}$  (Fig.9(b)) for the reaction  $^{48}\text{Ca} + ^{244}\text{Pu}$ . The dotted vertical line denotes the barrier height  $B_0$ , and the short dashed vertical line indicates the energy at the peak of  $D_{\text{eff}}$  which we call the most probable barrier height  $B_{\text{m.p.}}$ . From the dashed curve of Fig.9(a) one can see that the capture cross section goes down very sharply when the incident energy is lower than  $B_{\text{m.p.}}$ . This is because the decreasing slope of the left side of the weighting function  $D_{\text{eff}}$  is very steep due to strong closed shell effects ( $\gamma = 11.0$ ). In fact, one can find that the left side of the barrier distribution  $D_{\text{eff}}(B)$  is given by  $D_1(B)$  (see expression (19)), which becomes a  $\delta$ -function when  $\gamma \rightarrow \infty$ . For the system with  $\gamma$  much larger than 1 the effective barrier  $D_{\text{eff}}$  will have the similar behavior as is shown in Fig.9(b). Thus, the most probable barrier energy  $B_{\text{m.p.}}$  can be considered as the incident energy 'threshold', and for massive fusion reactions with  $\gamma$  much larger than 1 leading to superheavy nuclei such as  $^{48}\text{Ca}$  induced reactions, the suitable incident energy should be chosen in the region  $E_{\text{c.m.}} > B_{\text{m.p.}}$ . The barrier distribution for this case shown in Fig.9(b) looks like a  $\delta$ -function with a long tail in the high energy side. It seems to be that the Wong's formula with barrier height being the  $B_{\text{m.p.}}$  should work without introducing the  $\gamma$ . But the results calculated with Wong's formula and expression (17) are different especially at sub-barrier energies, as shown in Fig.9(a) (comparing the dot-dashed curve and the dashed curve). It seems to us that with this  $\gamma$  value like  $\gamma = 11.0$  the behavior of  $D_{\text{eff}}$  is still different from a  $\delta$ -function and the parameter  $\gamma$  still plays a role.

We find that the incident energies adopted in the experiments successfully producing superheavy nuclei in recent years [33, 34, 35, 36] for some reactions induced by  $^{48}\text{Ca}$  are very close the most probable barrier energies  $B_{\text{m.p.}}$ . Table 1 gives the comparison of the calculated most probable barrier energies  $B_{\text{m.p.}}$  with experimental incident energies  $E_{\text{min}}^{\text{exp}}$  used in recent years [33, 34, 35, 36] for some reactions induced by  $^{48}\text{Ca}$  leading to producing superheavy nuclei. The barrier height  $B_0$ , position  $R_0$  of the barrier, curvature at the top of

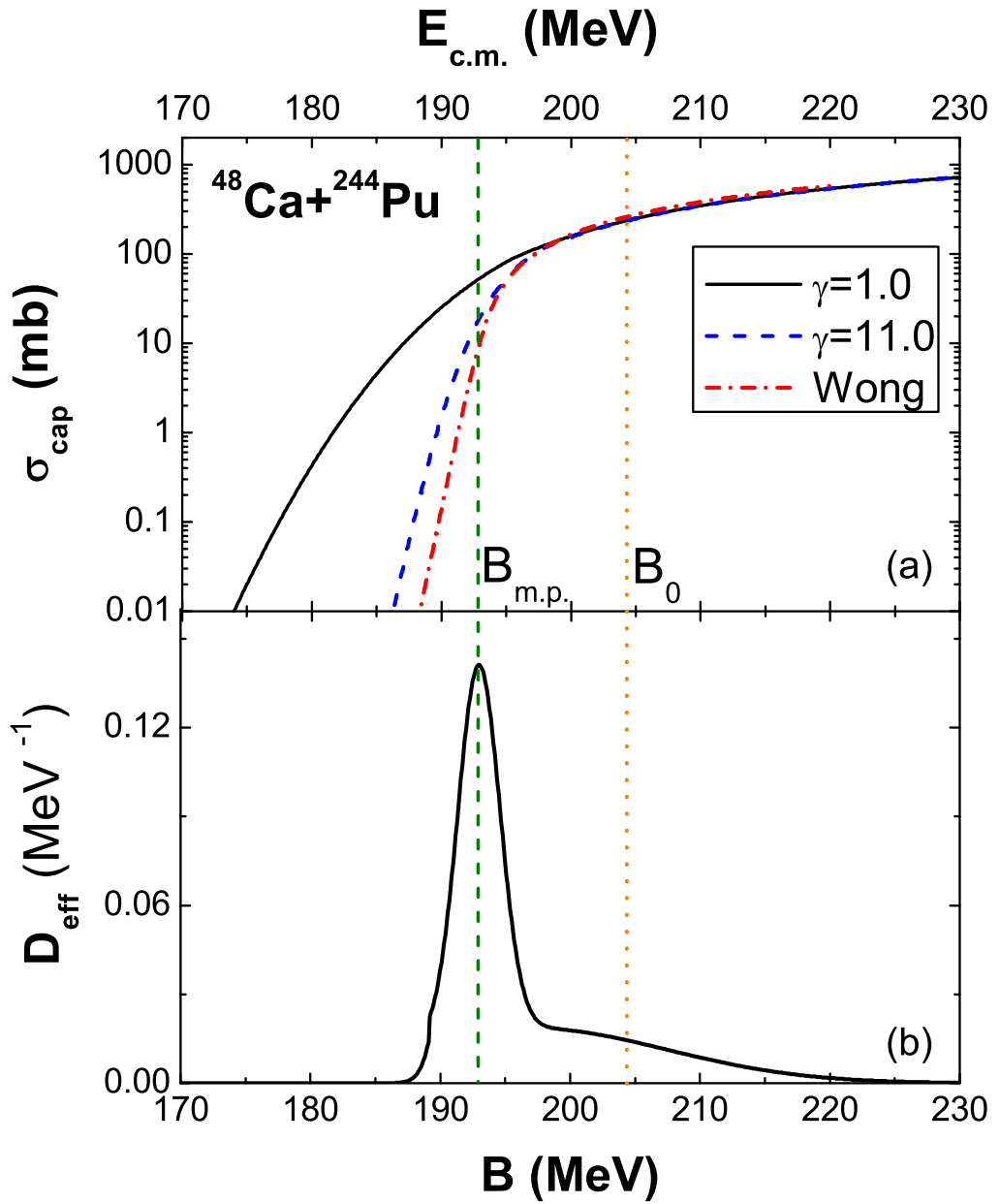


FIG. 9: (Color online) (a) Capture excitation function and (b) effective weighting function for the reaction  $^{48}\text{Ca} + ^{244}\text{Pu}$ . In (a) the solid and dashed curves show the results with  $\gamma = 1$  and with  $\gamma$  obtained by eq.(14), respectively. The dot-dashed curve denotes the results from Wong's formula with  $B = B_{\text{m.p.}}$ . The results in (b) are obtained by setting  $\gamma = 11.0$ .

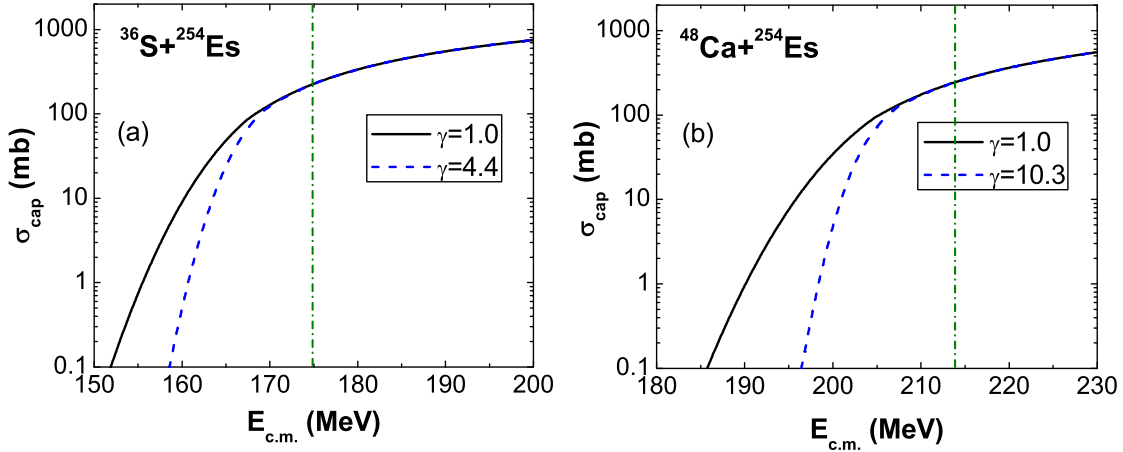


FIG. 10: (Color online) Capture excitation functions for the systems (a)  $^{36}\text{S}+^{254}\text{Es}$  and (b)  $^{48}\text{Ca}+^{254}\text{Es}$ .

the barrier expressed by  $\hbar\omega_0$ , factor  $\gamma$  are also listed. In addition, we list the mean value  $B_{\text{mean}}$  of the barrier height defined as

$$B_{\text{mean}} = \frac{\int B D_{\text{eff}}(B) dB}{\int D_{\text{eff}}(B) dB}. \quad (20)$$

The  $B_{\text{mean}}$  is, in general, larger than the  $B_{\text{m.p.}}$  since the slope of the left side of the weighting function  $D_{\text{eff}}$  is very steep. From the table one can find that for all listed reactions the energies  $E_{\text{min}}^{\text{exp}}$  are higher than the calculated most probable barrier energies  $B_{\text{m.p.}}$ , which supports our ideas about how to choose the favorable incident energy. Further, we find the experimental evaporation-residue excitation functions of the fusion reactions listed in Table 1 are peaked at the energies ranging from  $B_{\text{mean}}$  to  $B_0$  in most cases, which implies that the energy  $B_{\text{mean}}$  may be more suitable to be chosen as the incident beam energy in the fusion reactions with  $\gamma$  much larger than 1 for producing superheavy nuclei.

In addition to the reactions induced by  $^{48}\text{Ca}$  leading to superheavy nuclei, reactions with  $^{36}\text{S}$ ,  $^{37}\text{Cl}$ ,  $^{48}\text{Ca}$  and  $^{50}\text{Ti}$  bombarding on  $^{248}\text{Cm}$ ,  $^{247,249}\text{Bk}$ ,  $^{250,252,254}\text{Cf}$  and  $^{252,254}\text{Es}$  are also studied and all relevant parameters for the entrance-channel capture barriers for those fusion reactions are listed in Table 2. The table gives the Q-value for the reactions, the barrier height  $B_0$ , position  $R_0$  of the barrier, curvature at the top of the barrier expressed by  $\hbar\omega_0$ , factor  $\gamma$  of structure effects, the mean value  $B_{\text{mean}}$  of the barrier, the most probable barrier

TABLE I: The entrance-channel capture barriers of fusion reactions with  $^{48}\text{Ca}$  nuclei.

Reaction	$B_0(\text{MeV})$	$R_0(\text{fm})$	$\hbar\omega_0(\text{MeV})$	$\gamma$	$B_{\text{mean}}(\text{MeV})$	$B_{\text{m.p.}}(\text{MeV})$	$E_{\text{min}}^{\text{exp}}(\text{MeV})$
$^{48}\text{Ca} + ^{207}\text{Pb}$ [33]	183.37	12.0	4.44	8.9	176.28	173.18	173.3
$^{48}\text{Ca} + ^{208}\text{Pb}$ [33]	183.17	12.0	4.43	9.5	176.10	173.03	173.5
$^{48}\text{Ca} + ^{238}\text{U}$ [34]	200.82	12.25	4.19	10.7	193.09	189.71	191.1
$^{48}\text{Ca} + ^{242}\text{Pu}$ [34]	204.78	12.25	3.90	11.6	196.91	193.44	196
$^{48}\text{Ca} + ^{244}\text{Pu}$ [35]	204.31	12.25	3.99	11.0	196.44	192.99	193.3
$^{48}\text{Ca} + ^{243}\text{Am}$ [36]	206.87	12.25	3.87	9.8	198.89	195.39	207.1
$^{48}\text{Ca} + ^{245}\text{Cm}$ [35]	208.80	12.25	3.88	11.7	200.77	197.22	203
$^{48}\text{Ca} + ^{248}\text{Cm}$ [34]	208.25	12.25	3.89	10.8	200.23	196.71	198.6

energy  $B_{\text{m.p.}}$ , the excitation energy of compound nucleus  $E_{CN}^*$  when  $E_{\text{c.m.}} = B_{\text{mean}}$ , and the depth of capture pocket  $B_0 - B_s$  (or called quasi-fission barrier height[37], here  $B_s$  denotes the value at the bottom of the pocket, see Fig.1). Comparing the data from different reactions one can find that the reactions with  $^{37}\text{Cl}$  induce relatively higher excitation energies  $E_{CN}^*$  and those with  $^{48}\text{Ca}$  and  $^{50}\text{Ti}$  produce relatively lower excitation energies when  $E_{\text{c.m.}} = B_{\text{mean}}$ . So  $^{48}\text{Ca}$  and  $^{50}\text{Ti}$  induced reactions can be considered as good candidates of cold fusion reaction for producing superheavy nuclei from the point of a low excitation energy of the compound nuclei. Here we have not studied the orientation effect of deformed target, which has significant effect on fusion barrier height and the compactness of the fusion reactions. Recently, compactness of the  $^{48}\text{Ca}$  induced hot fusion reactions was studied in which it was shown that  $^{48}\text{Ca}$  induced reactions on various actinides were the best cold fusion reactions with optimum orientations of the hot fusion process[38]. By comparing the depths of the capture pockets for different reactions we find that the depth decreases with increase of the proton number of the projectile nuclei. We know that the shallower the pocket is, the stronger the quasi-fission is. So the projectile  $^{36}\text{S}$  inducing capture reactions is more favorable for the small quasi-fission probabilities of those reactions. By using this table we can easily calculate the capture cross sections by eqs.(15)–(17) for all reactions listed. Fig.10 shows the calculated capture excitation functions for the systems  $^{36}\text{S} + ^{254}\text{Es}$  and  $^{48}\text{Ca} + ^{254}\text{Es}$  with our approach by using the data from Table 2. In addition, the entrance-channel capture barriers of the reactions  $^{64}\text{Ni} + ^{238}\text{U}$ ,  $^{58}\text{Fe} + ^{244}\text{Pu}$ ,  $^{54}\text{Cr} + ^{248}\text{Cm}$  and  $^{50}\text{Ti} + ^{252}\text{Cf}$  which lead to the same

compound nucleus with  $Z = 120$  and  $N = 182$  are calculated and listed in Table 3. Table 2 and Table 3 provide us with very useful information for choosing an optimal combination of projectile and target and suitable incident beam energies for producing superheavy nuclei for unmeasured massive fusion reactions.

## V. CONCLUSION AND DISCUSSION

In this work, the Skyrme energy-density functional approach has been applied to study massive heavy-ion fusion reactions, especially those leading to superheavy nuclei. Based on the barriers calculated with the Skyrme energy-density functional, we propose the parameterized barrier distributions to effectively taken into account the multi-dimensional character of the realistic barrier. A large number of heavy-ion fusion reactions have been studied systematically. The average deviations of fusion cross sections at energies near and above the barriers from experimental data are less than 0.05 for 92% of 76 fusion reactions with  $Z_1Z_2 < 1200$ . Massive fusion reactions, for example, the  $^{238}\text{U}$ -induced reactions and the  $^{48}\text{Ca} + ^{208}\text{Pb}$  have been studied and their capture excitation functions have been reproduced well. The influence of the structure effects in the reaction partners on the capture cross sections are studied by using parameter  $\gamma$  in our model. To search the most favorable condition for the synthesis of superheavy nuclei, the optimal balance between the capture cross section and the excitation energy of the formed compound nuclei is studied by comparing the fusion reactions induced by the double-magic nucleus  $^{48}\text{Ca}$  and by  $^{32}\text{S}$  and  $^{35}\text{Cl}$ . Based on this study, the 'threshold-like' behavior of excitation function of capture cross sections with respect to incident beam energy has been explored and possible values of this 'threshold' for reactions mainly induced by  $^{48}\text{Ca}$  are given. Finally, we have further studied the capture reactions leading to superheavy nuclei such as  $^{36}\text{S}$ ,  $^{37}\text{Cl}$ ,  $^{48}\text{Ca}$  and  $^{50}\text{Ti}$  bombarding on  $^{248}\text{Cm}$ ,  $^{247,249}\text{Bk}$ ,  $^{250,252,254}\text{Cf}$  and  $^{252,254}\text{Es}$ , and as well as the reactions  $^{64}\text{Ni} + ^{238}\text{U}$ ,  $^{58}\text{Fe} + ^{244}\text{Pu}$ ,  $^{54}\text{Cr} + ^{248}\text{Cm}$  and  $^{50}\text{Ti} + ^{252}\text{Cf}$  which lead to the same compound nucleus with  $Z = 120$  and  $N = 182$ . The relevant parameters for calculating the capture cross section of these reactions have been provided which are helpful for the study of unmeasured massive fusion reactions. Especially, we predicted optimal fusion configuration and suitable incident beam energies for the synthesis of superheavy nuclei.

We notice that the deformation and orientation of colliding nuclei have a very significant role on fusion reactions. In [39, 40] the effect of deformation and orientation on the barrier

height and the compactness of fusion reactions were investigated systematically. However, this kind study is beyond the scope of present work. We have only made preliminary calculations of the potential barrier for  $^{48}\text{Ca} + ^{248}\text{Cm}$  with the deformation and orientation of  $^{248}\text{Cm}$  taken into account in the entrance channel. For this reaction the lowest barrier is obtained for the orientation  $\Theta = 0^\circ$ , i.e. when  $^{48}\text{Ca}$  touches the tip of deformed  $^{248}\text{Cm}$  target, while the highest barrier is obtained for  $\Theta = 90^\circ$ , when  $^{48}\text{Ca}$  touches the side. The lowest barrier obtained for  $\Theta = 0^\circ$  is a little bit lower than the most probable barrier height  $B_{\text{m.p.}}$  of this reaction given in Table 1 and the barrier distribution due to the orientation of  $^{248}\text{Cm}$  is close to the effective weighting function  $D_{\text{eff}}(B)$  which is for describing the capture process of the reaction if assuming the orientation probability decreases gradually from  $0^\circ$  to  $90^\circ$ . So the deformation effects seem to be partly involved in the parameterized barrier distribution functions. The study on this aspect is in progress.

## I. ACKNOWLEDGEMENTS

This work is supported by Alexander von Humboldt Foundation and National Natural Science Foundation of China, No. 10235030, 10235020. Wang is grateful to Prof. Enguang Zhao and Prof. Junqing Li for fruitful discussions.

---

[1] C.Y.Wong, Rev. Lett. **31**, 766 (1973).

[2] K. Hagino, N. Rowley, and A. T. Kruppa, Comput. Phys. Commun. **123**, 143 (1999).

[3] J. O. Newton, R. D. Butt, M. Dasgupta et al., Phys. Rev. C **70**, 024605 (2004).

[4] K. Siwek-Wilczynska and J. Wilczynski, Phys. Rev. C **69**, 024611 (2004).

[5] M. Liu, N. Wang, Z. Li, X. Wu and E. Zhao, Nucl. Phys. A **768**, 80 (2006).

[6] M. Brack, C. Guet, H.-B. Hakanson, Phys. Rep. **123**, 275 (1985).

[7] M. Trotta, A.M. Stefanini, L. Corradi et al. Phys. Rev. C **65**, 011601 (2001).

[8] F. Scarlassara, G. Montagnoli, et al. Prog. Theor. Phys. Suppl. No. **154**, 31 (2004).

[9] Zhang Huan-Qiao, et al. Chin. Phys. Lett. **22**, 3048 (2005).

[10] Yu. Ts. Oganessian, V. K. Utyonkov, Yu. V. Lobanov, et. al., Phys. Rev. C **62**, 041604 (2000); Phys. Rev. C **63**, 011301 (2000).

[11] V.Yu. Denisov and W. Noerenberg, Eur. Phys. J. **A15**, 375 (2002).

[12] R.Bass, Nucl. Phys. A **231**, 45 (1974).

[13] D. Vautherin, D.M. Brink, Phys. Rev. C **5**, 626 (1972).

[14] J. Bartel and K. Bencheikh, Eur. Phys. J. **A14**, 179 (2002).

[15] J. Bartel, M. Brack and M. Durand, Nucl. Phys. A **445**, 263 (1985).

[16] B. Grammaticos, Z. Phys. A **305** 257 (1982).

[17] P. Hohenberg, W. Kohn, Phys. Rev. **136**, B864(1964).

[18] W. D. Myers, W. J. Swiatecki, Phys. Rev. C **62**, 044610 (2000).

[19] P.H.Stelson, Phys. Lett. B **205**, 190 (1988).

[20] J.R. Leigh, M. Dasgupta and D.J. Hinde, Phys. Rev. C **52**, 3151 (1995).

[21] J.O. Newton, C.R. Morton and M. Dasgupta, Phys. Rev. C **64**, 64608 (2001).

[22] F.L.H. Wolfs, R.V.F. Janssens, R. Holzmann et al., Phys. Rev. C **39** 865 (1989).

[23] W.Q. Shen, J. Albinski, A. Gobbi et al. Phys. Rev. C **36**, 115 (1987).

[24] J. Toke, R.Bock, et al., Phys. Lett. B **142**, 258 (1984).

[25] E.V.Prokhorova, E.A.Cherepanov, M.G.Itkis, et al, arXiv:nucl-ex/0309021.

[26] A.J. Pacheco, J.O Fernandez Niello, D.E DiGregorio et al., Phys. Rev. C **45**, 2861 (1992).

[27] G. Audi and A. H. Wapstra, Nucl. Phys. A **595**, 409 (1995).

[28] P. Moller, J. R. Nix, W. D. Myers, W. J. Swiatecki At. Data and Nucl. Data Tables **59**, 185

(1995).

- [29] H. Timmers, D. Ackermann, et al., Nucl. Phys. **A 633**, 421 (1998); and the doctoral thesis of H. Timmers.
- [30] P.R.S. Gomes, I.C. Charret and R. Wanis, Phys. Rev. C **49**, 245 (1994).
- [31] C.R. Morton, A.C. Berriman and M. Dasgupta, Phys. Rev. C **60**, 044608 (1999).
- [32] D. Boilley, Y. Abe, and J.-D. Bao, Eur. Phys. J. A **18**, 627 (2003).
- [33] Yu.Ts. Oganessian, V.K. Utyonkov, Yu.V. Lobanov et al., Phys. Rev. C **64**, 054606 (2001).
- [34] Yu.Ts. Oganessian, V.K. Utyonkov, Yu.V. Lobanov et al., Phys. Rev. C **70**, 064609 (2004).
- [35] Yu.Ts. Oganessian, V.K. Utyonkov, Yu.V. Lobanov et al., Phys. Rev. C **69**, 054607 (2004).
- [36] Yu.Ts. Oganessian, V.K. Utyonkov, Yu.V. Lobanov et al., Phys. Rev. C **69**, 021601 (2004).
- [37] G.G.Adamian, N.V. Antonenko, W.Scheid and V.V.Volkov, Nucl.Phys. A **627**, 361 (1997).
- [38] Raj K. Gupta, M. Manhas, W. Greiner, Phys. Rev. C **73**, 054307 (2006).
- [39] A. Iwamoto, P. Möller, J. R. Nix, H. sagawa, Nucl. Phys. A **596**, 329 (1996).
- [40] Raj K. Gupta, et.al. J. Phys. G: Nucl. Phys. **31**, 631 (2005).

TABLE II: The entrance-channel capture barriers for fusion reactions with  $^{36}\text{S}$ ,  $^{37}\text{Cl}$ ,  $^{48}\text{Ca}$  and  $^{50}\text{Ti}$  bombarding on  $^{248}\text{Cm}$ ,  $^{247,249}\text{Bk}$ ,  $^{250,252,254}\text{Cf}$  and  $^{252,254}\text{Es}$ .

Reaction	Q(MeV)	$B_0(\text{MeV})$	$R_0(\text{fm})$	$\hbar\omega_0(\text{MeV})$	$\gamma$	$B_{\text{mean}}(\text{MeV})$	$B_{\text{m.p.}}(\text{MeV})$	$E_{CN}^*(\text{MeV})$	$B_0 - B_s$
$^{36}\text{S} + ^{248}\text{Cm}$	-122.05	170.45	12.0	4.34	5.3	163.75	161.00	41.70	8.72
$^{36}\text{S} + ^{247}\text{Bk}$	-126.30	172.60	12.0	4.33	4.7	165.78	163.10	39.48	8.43
$^{36}\text{S} + ^{249}\text{Bk}$	-124.58	172.03	12.0	4.23	3.9	165.18	162.58	40.60	8.23
$^{36}\text{S} + ^{250}\text{Cf}$	-127.14	174.04	12.0	4.29	6.2	167.24	164.37	40.10	8.27
$^{36}\text{S} + ^{252}\text{Cf}$	-125.00	173.53	12.0	4.23	5.1	166.70	163.89	41.70	8.41
$^{36}\text{S} + ^{254}\text{Cf}$	-122.48	173.02	12.0	4.17	3.9	166.13	163.51	43.65	8.49
$^{36}\text{S} + ^{252}\text{Es}$	-128.84	175.36	12.0	4.23	5.4	168.47	165.65	39.63	8.18
$^{36}\text{S} + ^{254}\text{Es}$	-126.81	174.97	12.0	4.17	4.4	168.04	165.26	41.23	8.25
$^{37}\text{Cl} + ^{248}\text{Cm}$	-128.14	180.65	12.25	4.58	3.0	173.37	170.66	45.23	7.86
$^{37}\text{Cl} + ^{247}\text{Bk}$	-131.56	182.90	12.0	4.25	2.8	175.50	172.83	43.94	7.46
$^{37}\text{Cl} + ^{249}\text{Bk}$	-129.56	182.60	12.25	4.54	1.8	175.03	172.61	45.47	7.59
$^{37}\text{Cl} + ^{250}\text{Cf}$	-134.39	184.45	12.25	4.55	4.1	177.12	174.28	42.73	7.35
$^{37}\text{Cl} + ^{252}\text{Cf}$	-131.94	184.03	12.25	4.54	2.9	176.60	173.87	44.65	7.56
$^{37}\text{Cl} + ^{254}\text{Cf}$	-129.40	183.57	12.25	4.52	1.6	175.91	173.53	46.52	7.74
$^{37}\text{Cl} + ^{252}\text{Es}$	-135.20	185.96	12.25	4.54	3.5	178.51	175.70	43.31	7.23
$^{37}\text{Cl} + ^{254}\text{Es}$	-132.96	185.62	12.25	4.52	2.4	178.04	175.44	45.08	7.41
$^{48}\text{Ca} + ^{248}\text{Cm}$	-167.27	208.25	12.25	3.89	10.8	200.23	196.71	32.96	5.46
$^{48}\text{Ca} + ^{247}\text{Bk}$	-171.71	210.80	12.25	3.95	9.6	202.67	199.11	30.95	5.27
$^{48}\text{Ca} + ^{249}\text{Bk}$	-170.76	210.46	12.25	3.83	9.1	202.33	198.76	31.57	5.30
$^{48}\text{Ca} + ^{250}\text{Cf}$	-174.53	212.56	12.25	3.66	11.4	204.39	200.81	29.86	5.11
$^{48}\text{Ca} + ^{252}\text{Cf}$	-173.77	212.10	12.5	4.41	11.0	203.94	200.37	30.17	5.17
$^{48}\text{Ca} + ^{254}\text{Cf}$	-173.28	211.63	12.5	4.38	10.7	203.48	199.92	30.20	5.25
$^{48}\text{Ca} + ^{252}\text{Es}$	-177.43	214.29	12.5	4.43	10.6	206.04	202.39	28.61	4.98
$^{48}\text{Ca} + ^{254}\text{Es}$	-176.97	213.94	12.5	4.39	10.3	205.70	202.13	28.73	5.05

Reaction	Q(MeV)	B <sub>0</sub> (MeV)	R <sub>0</sub> (fm)	ħω <sub>0</sub> (MeV)	γ	B <sub>mean</sub> (MeV)	B <sub>m.p.</sub> (MeV)	E <sub>CN</sub> <sup>*</sup> (MeV)	B <sub>0</sub> -B <sub>s</sub>
<sup>50</sup> Ti+ <sup>248</sup> Cm	-185.52	229.00	12.25	3.75	3.9	219.88	216.39	34.36	4.41
<sup>50</sup> Ti+ <sup>247</sup> Bk	-191.42	231.85	12.25	3.80	4.1	222.63	219.00	31.21	4.14
<sup>50</sup> Ti+ <sup>249</sup> Bk	-189.78	231.45	12.25	3.67	3.3	222.16	218.71	32.38	4.18
<sup>50</sup> Ti+ <sup>250</sup> Cf	-194.40	233.79	12.25	3.64	4.9	224.56	220.84	30.16	3.98
<sup>50</sup> Ti+ <sup>252</sup> Cf	-193.02	233.23	12.25	3.53	4.2	223.97	220.33	30.95	3.96
<sup>50</sup> Ti+ <sup>254</sup> Cf	-191.92	232.67	12.5	4.38	3.6	223.38	219.81	31.46	3.97
<sup>50</sup> Ti+ <sup>252</sup> Es	-197.90	235.72	12.25	3.52	4.3	226.37	222.67	28.47	3.71
<sup>50</sup> Ti+ <sup>254</sup> Es	-196.81	235.24	12.5	4.39	3.8	225.86	222.21	29.05	3.69

TABLE III: The same as Table 2, but for reactions <sup>64</sup>Ni+<sup>238</sup>U, <sup>58</sup>Fe+<sup>244</sup>Pu, <sup>54</sup>Cr+<sup>248</sup>Cm and <sup>50</sup>Ti+<sup>252</sup>Cf.

Reaction	Q(MeV)	B <sub>0</sub> (MeV)	R <sub>0</sub> (fm)	ħω <sub>0</sub> (MeV)	γ	B <sub>mean</sub> (MeV)	B <sub>m.p.</sub> (MeV)	E <sub>CN</sub> <sup>*</sup> (MeV)	B <sub>0</sub> -B <sub>s</sub>
<sup>64</sup> Ni+ <sup>238</sup> U	-237.41	276.01	12.5	4.61	7.1	265.26	260.73	27.85	1.79
<sup>58</sup> Fe+ <sup>244</sup> Pu	-219.97	262.88	12.25	3.93	1.0	251.56	248.80	31.60	2.56
<sup>54</sup> Cr+ <sup>248</sup> Cm	-207.16	248.52	12.25	4.20	3.0	238.51	234.86	31.35	3.26
<sup>50</sup> Ti+ <sup>252</sup> Cf	-193.02	233.23	12.25	3.53	4.2	223.97	220.33	30.95	3.96